Dark Mass is Potential Energy

Nicolas Poupart, Independent Researcher (2025)
99 Chemin Scraire, Mille-Isles, Québec, Canada (J0R 1A0)
(450) 939-2167
nicolas.poupart@yahoo.fr

Abstract *— This paper demonstrates that gravitational potential energy ($E = -GmM / d$) accounts for the phenomenon commonly attributed to dark matter, by applying the mass-energy equivalence relation ($E = mc^2$). No additional assumptions are made beyond the principle of volume conservation, ensuring that the gravitational field remains conservative and uninfluenced by forces other than gravity. We develop a straightforward equation and algorithm to accurately compute the potential energy of a stellar system. The theoretical implications of this model are explored with respect to energy production by various types of stars and black holes in galaxies. The model is empirically tested against the SPARC database comprising 175 galaxies to assess its validity. We derive the logical consequences of the potential energy stored in the gravitational field; a claim validated by SPARC data. The final consequence is the production of dark energy and the reproduction of ΛCDM cosmology. We conclude by demonstrating that the experimental adequacy of our model is 7.5σ.*

Introduction

Since Vera Rubin postulated the existence of galactic dark mass to explain the flatness of galactic rotation curves (1; 2; 3), no convincing explanation for the nature of this mass has been provided. Attempts to attribute the missing mass to undetectable baryonic matter were largely refuted by the AGAPE (4), MACHO (5), and EROS (6) programs. Similar explanations involving non-baryonic or exotic particles have also failed to account for the discrepancy. Numerous detection efforts, including those by the LUX (7), PICASSO (8), PICO (9), and SuperCDMS (10) collaborations, have thus far been unsuccessful. Likewise, results from CERN's latest accelerator suggest that physics remains consistent with the Standard Model, making the existence of exotic particles increasingly unlikely. It also remains extremely difficult to explain this phenomenon using current gravitational theory, whether Newtonian gravitation or general relativity.

In cosmology, the prevailing framework is the ΛCDM model, which postulates the existence of cold dark matter. For most physicists, the concept of mass remains inseparable from that of matter. Moreover, the term "dark matter" is often used categorically, although it more accurately refers to "dark mass." One alternative to the existence of real dark mass is to modify gravitation at galactic scales. However, such efforts are challenged by the remarkable empirical adequacy of general relativity in describing observed phenomena and the inferred presence of dark mass (11; 12; 13).

The explanation proposed in this article takes a fundamentally different approach. Dark mass is neither a form of real matter nor the result of modified gravitation. Rather, it is a secondary effect inherent to the current formulation of gravitational theory—specifically, the gravitational potential energy stored in the gravitational field. The only axioms employed are $E = -GmM / d$ and $E = mc^2$. Thus, the explanation relies solely on the judicious application of classical physics.

Useful Gravitational Potential Energy

If we consider the Newtonian gravitational force equation, $F = GmM / d^2$, we obtain—by integrating from d to infinity—the potential energy formula $E_p = -GmM / d$. While this formulation yields negative potential energy which can be used for calculating the motion of celestial bodies, it is unsuitable for evaluating the total physical potential energy of a system.

To determine the physically meaningful potential energy, we must compute the energy difference between two states of the system—analogous to lifting a mass m from position d by a height h. In such a case $\Delta E_p = E_p(d + h) - E_p(d) = GmMh / (d^2 + dh)$. This expression represents the *usable* form of gravitational potential energy. The concept of absolute negative energy E_p is not directly interpretable in physical terms.

However, this formulation becomes impractical for systems involving two celestial bodies (e.g., planets, stars, or galaxies), because the initial reference distance d is undefined or ambiguous. To resolve this, we compute the energy difference between a compact state—a single solid spherical mass $M_t = m + M$ and a configuration of two distinct spherical bodies, m and M, separated by a distance d.

Let the two bodies have radii r and R, and volumes $v = 4\pi r^3/3$ and $V = 4\pi R^3/3$, with corresponding densities m/v and M/V. The total volume of the single solid sphere is $V_t = V + v = 4\pi/3\ (R^3 + r^3)$, and its radius $R_t = (R^3 + r^3)^{1/3}$. Assuming equal volumetric densities, $m/v = M/V$, that of the single compact ball will be identical $m/v = M/V = M_t/V_t$; if not, it assumes an average density weighted by the contributions of m and M.

The gravitational potential energy of a homogeneous solid sphere is given by $E_p = -3GM^2 / 5R$. The gravitational potential energy of the system can be evaluated by comparing the initial state (a single compact mass), the final state (two separated masses), and the difference between them:

$$E_i = -\frac{3GM_t^2}{5R_t}$$

$$E_f = -\frac{3GM^2}{5R} - \frac{3Gm^2}{5r} - \frac{GMm}{d}$$

$$\Delta E_p = E_f - E_i = \left(-\frac{3GM^2}{5R} - \frac{3Gm^2}{5r} - \frac{GMm}{d}\right) + \frac{3GM_t^2}{5R_t}$$

This expression quantifies the energy change from a compact configuration to a system of two separated masses. It represents a redistribution of matter that preserves the original component densities, thereby ensuring that the transformation involves only gravitational forces.

Gravitational Potential Energy is Massive

Gravitational potential energy can be expressed as $E_p = m_p c^2$, indicating that it must be stored as mass within the system. This statement is readily illustrated through a simple thought experiment. Consider a nuclear reactor that converts a mass m_n into electrical energy, which is then used to raise a mass m to a height h.

There should be no debate regarding whether the Earth's mass remains unchanged before and after the transformation. Given the conservation of mass-energy m_n within the Earth system, general relativity ensures that its gravitational field remains unchanged. The question of whether this constitutes “real” mass is meaningless, since mass is defined by its measurable gravitational or inertial effects. However, this new mass does not in turn generate potential energy ad infinitum; if such a principle of self-induction exists in the field, the Newtonian calculation is simply the limiting sum.

Moreover, since the equivalence of inertial and gravitational mass has never been empirically violated (14), we may, for now, treat gravitational potential energy as fully equivalent to its mass representation.

Calculation of the Potential Energy of Celestial Bodies

	***m* (kg)**	***M* (kg)**	***r* (m)**	***R* (m)**	***d* (m)**	***R*$_t$ (m)**
Moon + Earth	7.348E+22	5.972E+24	1.738E+06	6.378E+06	3.844E+08	6.421E+06
Earth + Sun	5.972E+24	1.989E+30	6.378E+06	6.963E+08	1.496E+11	6.963E+08
Jupiter + Sun	1.898E+27	1.989E+30	6.991E+07	6.963E+08	7.780E+11	6.966E+08
Sun + M80	1.989E+30	9.985E+35	6.963E+08	5.534217E+10	4.541E+17	5.534221E+10
Sun + Galaxy	1.989E+30	5.000E+40	6.963E+08	2.040E+12	5.000E+20	2.040E+12

This table contains the standard values for the celestial bodies under consideration, except for the radii for the globular cluster M80 and a representative galaxy (indicated by gray boxes). We modeled the initial state as a solid sphere of mass $M + m$, assuming solar density. The final state is the sun at distance d of a mass M of solar density. For the Sun–galaxy pair, the values used are, $R = 2.0398571210655 \times 10^{12}$ and $R_t = 2.0398571213359 \times 10^{12}$. The

rationale behind this construction will be addressed in a subsequent section. In either case, the radius is calculated using the relation $R_t = (R^3 + r^3)^{1/3}$.

	E_i (j)	E_f (j)	ΔE_p (j)	ΔE_p (kg)	$m / \Delta E_p$
Moon + Earth	-2.2795E+32	-2.2413E+32	3.8176E+30	4.2477E+13	0.000000001
Earth + Sun	-2.2751E+41	-2.2751E+41	1.3024E+36	1.4491E+19	0.000002427
Jupiter + Sun	-2.2787E+41	-2.2751E+41	3.5519E+38	3.9520E+21	0.000002082
Sun + M80	-7.2141E+50	-7.2141E+50	2.3949E+45	2.6647E+28	0.013396966
Sun + Galaxy	-4.9079E+58	-4.9079E+58	3.2540E+48	3.6206E+31	18.20

The table presents the gravitational potential energy differences between current physical configurations and their hypothetical fusion into a single mass. For context, the complete annihilation of one kilogram of matter yields an energy output approximately equivalent to that of a hydrogen bomb. For example, 2 kg of deuterium fused with 3 kg of tritium results in a mass loss of roughly 1 kg—comparable to the energy released by the Tsar Bomba.

Based on this equivalence, the merger of the Moon with the Earth would release energy equivalent to approximately 40 trillion hydrogen bombs. This potential energy corresponds to a mass of about 40 billion metric tons—a value that is far from negligible.

If we consider the energy released by merging the Earth into the Sun, the resulting energy would correspond to over 14 million billion metric tons. However, this value is still less than the mass the Sun loses each hour due to nuclear fusion. Depending on its spatial distribution, this energy-equivalent mass could, in principle, be measurable.

If we examine the ratio $m/\Delta E_p$, representing the mass of the smaller body relative to the potential energy of the system, we find that it is negligible in most cases—except at the galactic scale, where it approaches the order of magnitude of the observed dark mass ratio.

The Potential Energy of Celestial Systems

The first observation is that the term $-GmM / d$ of ΔE_p is negligible at all relevant scales, where $d \gg R \gg r$. This result is intuitive from a physical standpoint, altering the distance between two celestial bodies, such as the Earth and the Moon, leads to minimal changes in gravitational energy compared to the energy released by their hypothetical fusion. This approximation holds across all celestial systems.

The energy expression thus simplifies to:

$$\Delta E_p = \frac{3G}{5}\left(\frac{M_t^2}{R_t} - \frac{M^2}{R} - \frac{m^2}{r}\right)$$

This implies that the spatial arrangement of bodies relative to one another is irrelevant for calculating total gravitational potential energy. If we consider a system of n masses m_i with radii r_i, merged sequentially, we obtain the following expressions $M_i = \sum_{j \le i} m_j$, $R_i = (R_{i-1}^3 + r_i^3)^{1/3}$ and

$$\Delta E_i = \frac{3G}{5}\left(\frac{M_i^2}{R_i} - \frac{M_{i-1}^2}{R_{i-1}} - \frac{m_i^2}{r_i}\right), \Delta E_p = \sum_{i \le n} \Delta E_i$$

It is important to note that the order of mergers is irrelevant, as the gravitational field is conservative.

Simplified Calculation with Identical Mass and Radius

By assuming identical mass m and radius r for each of the n bodies, the calculation simplifies considerably. In this case, the cumulative mass at the i^{th} merger step is $M_i = im$, and the corresponding radius is:

$$\frac{M_i}{V_i} = \frac{m}{v} \quad \Rightarrow \quad R_i = \left(\frac{M_i r^3}{m}\right)^{1/3}$$

since M_i retains the same density as the original body of mass m.

The change in gravitational potential energy at each step is given by:

$$\Delta E_i = \frac{3G}{5}\left(\frac{M_i^2}{R_i} - \frac{M_{i-1}^2}{R_{i-1}} - \frac{m^2}{r}\right), \Delta E_p = \sum_{i \le n} \Delta E_i$$

Due to cancellation of intermediate terms, the telescoping sum simplifies to:

$$\Delta E_p = \frac{3G}{5}\left(\frac{M_n^2}{R_n} - n\frac{m^2}{r}\right)$$

Since $M_n = nm$, we find:

$$M_n^2 = n^2 m^2 \quad \text{and} \quad R_n = \left(\frac{M_n r^3}{m}\right)^{1/3} = n^{1/3} r$$

Substituting into the equation:

$$\Delta E_p = \frac{3G}{5}\left(\frac{n^2 m^2}{n^{1/3} r} - \frac{n m^2}{r}\right) = \frac{3G}{5}\left(n^{5/3} - n\right)\frac{m^2}{r}$$

This final expression shows that the total gravitational potential energy of the system depends solely on the mass, radius, and number of individual bodies. Consequently, a small radius and large mass—i.e., high density—of the component solid spheres significantly increases the total potential energy of the system.

Practical Estimation from a Stellar Population Histogram

In practice, the stellar population of a galaxy is typically known through a mass distribution histogram. The total stellar mass M can be partitioned into k discrete mass intervals, each denoted by a triplet (M_i, m_i, r_i), $M_i = n_i m_i$ representing the cumulative mass, individual stellar mass and stellar radius respectively.

The first step involves calculating the contribution from each interval as:

$$\Delta E_{\text{pa}} = \sum_{i \le k} \frac{3G}{5}\left(\frac{M_i^2}{R_i} - n_i \frac{m_i^2}{r_i}\right), R_i = \left(\frac{M_i r_i^3}{m_i}\right)^{1/3}$$

where R_i is the radius associated with mass M_i, and n_i is the number of stars of mass m_i in interval i.

Next, we compute the residual potential energy ΔE_{pb} by merging all k compact balls (M_i, R_i). The total gravitational potential energy of the system is then:

$$\Delta E_p = \Delta E_{pa} + \Delta E_{pb}$$

Alternatively, this process can be formalized via a function $f(m, r, M, M_i, R_i) \mapsto (\Delta E_p, M_t, R_t)$ which takes as input the mass m, radius r, and total mass M of the stellar units, along with an optional compact configuration (M_i, R_i) that may be initialized to zero. The function returns the total potential energy for the interval ΔE_{pi}, along with the updated total mass M_t and radius R_t, $\Delta E_p = \Delta E_p + \Delta E_{pi}$. The algorithm is simply:

$f(m, r, M, M_i, R_i) \mapsto (\Delta E_{pi}, M_t, R_t)$:

$n = M$ / m

$M_t = M + M_i$

$R = n^{1/3} r$

$R_t = (R^3 + R_i^3)^{1/3}$

$\Delta E_{pi} = (3G/5)\,[M_t^2/\, R_t - n\, m^2/\, r]$

Hierarchical Computation of Gravitational Potential Energy

To calculate the gravitational potential energy ΔE_p of larger-scale structures—such as galaxy clusters or superclusters—each constituent galaxy must first be reduced to a compact configuration using the previously described method. This process yields three key quantities for each galaxy: the potential energy ΔE_p, the total mass M_t, and the radius R_t. The total mass of the resulting compact object is then given by $M = M_t + \Delta E_p / c^2$ where $\Delta E_p / c^2$ accounts for the mass-equivalent of the stored gravitational potential energy. The radius R of this composite object is now that of the galaxy with the dark mass distributed in the gravitational field.

This merging procedure can then be reapplied at the next hierarchical scale, considering each galaxy as a single unit within a larger gravitational system, whether a cluster or a supercluster. As will be demonstrated in the dark energy section, only density matters so the radius of the solid sphere must be selected to simply respect the galactic mass density.

Treatment of Galactic Gas in Gravitational Potential Energy Calculations

Galactic gas poses a particular modeling challenge because it does not form distinct compact objects, making direct gravitational fusion calculations inapplicable as such. However, it is well established that the gas possesses a gravitational potential energy at least equivalent to that of the stellar component, since it constitutes the raw material for the gravitational collapse processes leading to star formation.

Because of its very low density, it is possible to consider each gas molecule of mass m as practically isolated, which amounts to assuming that the average distance between molecules tends to infinity. If we model the collapse of this gas into a compact stellar configuration of mass M_i, the conservative transport of molecules in this configuration must respect volume conservation. We then have:

$$\frac{M_i}{V_i} = \frac{m}{v} \quad \Rightarrow \quad R_i = \left(\frac{M_i r^3}{m}\right)^{1/3}$$

Since the field is conservative and the fusion order can be arbitrary and the system must respect the principle of reversibility, the only possibility is to consider that the density is respected and therefore that the gas has in the initial state the same density as the stellar configuration. Therefore, the gas must be considered as contributing indistinguishably to the stellar mass distribution. This modeling assumption is corroborated by our numerical tests and is necessary to minimize errors in the interpretation of observational data.

The Initial Compact Ball Problem

We define the initial compact configuration as a solid sphere that conserves the total volume of the bodies it replaces. This strict conservation of volume ensures the physical consistency of the state of matter before and after compaction. Given the difference in potential energy between a final dilute state and an initial compact state, it is possible to simplify this expression:

$$\Delta E_p = \frac{3G}{5}\left(\frac{M_n^2}{R_n} - n\frac{m^2}{r}\right)$$

Assuming $M_n = nm$, we have:

$$M_n^2 = n^2 m^2 \quad \text{and} \quad R_n = \left(\frac{M_n r^3}{m}\right)^{1/3} = n^{1/3} r$$

Substituting into the equation:

$$\Delta E_p = \frac{3G}{5}\left(\frac{n^2 m^2}{n^{1/3} r} - \frac{n m^2}{r}\right) = \frac{3G}{5}\left(n^{5/3} - n\right)\frac{m^2}{r}$$

The asymptotic behavior shows that for $n >> 1$, the $n^{5/3}$ term dominates over n, justifying the approximation:

$$\Delta E_p \approx \frac{3G}{5} \cdot \frac{M_n^2}{R_n}$$

Therefore, the potential energy of the dilute structure is strictly equivalent to that of the compact structure. Thus, if the compact ball M_n, or a corresponding dilute system, collapses into a black hole, its potential energy ΔE_p will be entirely emitted in radiation. Indeed, the final black hole of mass M_n has no potential energy in the classical sense and is entirely defined by its mass, spin, and charge. The transition from the compact ball to the black hole therefore requires the loss of its potential energy. We can therefore distinguish two types of energy regime, those whose critical mass will necessarily push it to collapse into a black hole and the others. Thus, the ratio E_{rad} / ΔE_p of the radiation emission of a kilo of sand collapsing into a compact ball will be practically zero while that of the hypothetical collapse of a galaxy is strictly equal to one.

The compact solid sphere, conserving volumes, is the state of maximum entropy of maximum energy while the black hole is the state of maximum entropy of minimum energy.

The fact that the compact ball conserving volumes corresponds to the state of maximum total potential energy is simply the consequence of the action-reaction principle and the conservation of energy.

This is the most compact state that does not introduce additional repulsive forces, such as degeneracy pressure or radiation pressure, which did not exist in the initial diluted state. It is enough to imagine this compact ball as simply being, for example, all the stars of a galaxy placed side by side. In such a configuration, all the initial forces are conserved. This conservation of forces is strictly necessary to keep the total energy of the system intact.

Theoretical Model

We apply our gravitational potential energy theory to generate theoretical models in the form of curves, representing the dark mass ratio produced by galaxies with varying numbers of stars. Each curve corresponds to a different galaxy size (Figures 1 and 2).

The x-axis represents the stellar mass M_S, expressed in solar masses, of the stars of the galaxy. Stellar radii are determined using the standard mass–radius relationship for main-sequence stars ($R \propto M^{0.8}$ if $M < M_\odot$, $R \propto M^{0.57}$ otherwise). The y-axis shows the ratio of total gravitationally induced dark mass M_G to the total baryonic stellar mass M_B, that is, M_G / M_B.

For example, a galaxy with 100 billion stars (thin dotted line) yields a dark mass ratio of approximately 28 when all the stars have 1 $M_\odot$ and 1 $R_\odot$. A population of 200 billion stars yields a ratio of 45, and 300 billion stars results in a ratio of 60. These values exceed the commonly accepted ratio of around 20 for the Milky Way.

Nevertheless, the order of magnitude is consistent, despite the extreme simplification of this analysis. This result reinforces the central hypothesis that dark mass is not a distinct form of matter but rather emerges from the gravitational potential energy of the system.

Impact of Stellar Density Variations on Dark Mass Production

The inclusion of less dense stars, such as red giants, significantly reduces the modeled production of gravitationally induced dark mass (Figures 3 and 4). This scenario is based on the same stellar population used in previous cases, composed primarily of stars with 1 $M_\odot$ and 1 $R_\odot$, to which a variable fraction of red giants is added, each with 4 $M_\odot$ and 100 $R_\odot$. The resulting decrease in average stellar density lowers the total gravitational potential energy of the system and, consequently, the dark mass ratio.

Conversely, the addition of dense stellar remnants, such as white dwarfs (0.6 $M_\odot$, 0.0085 $R_\odot$) and neutron stars (1.35 $M_\odot$, 10.8 km), leads to a dramatic increase in dark mass production (Figures 5 and 6). The extremely high densities of these objects substantially elevate the system's total potential energy. In realistic stellar populations, however, this increase is moderated by the presence of low-density stars (e.g., red giants) and black holes.

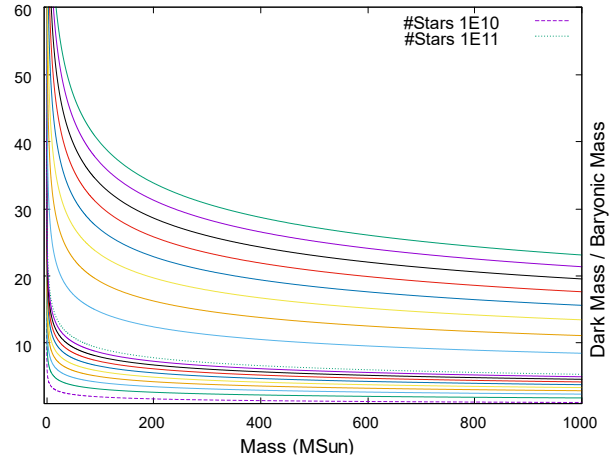

Figure 1

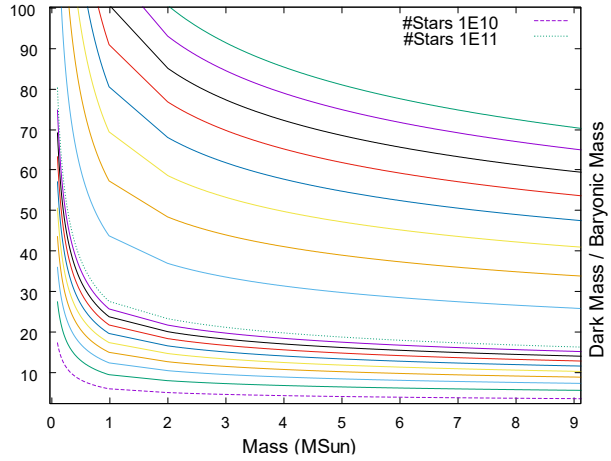

Figure 2

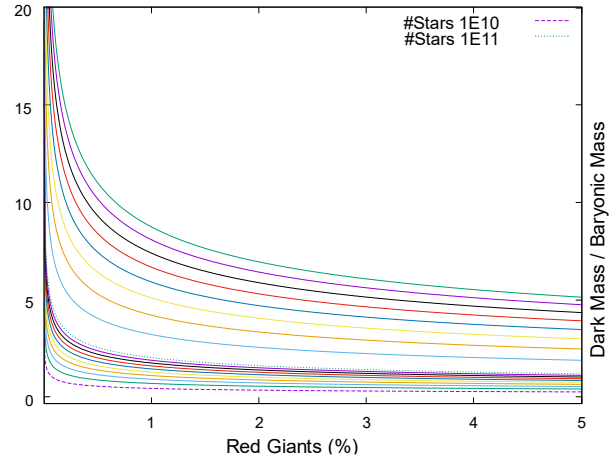

Figure 3

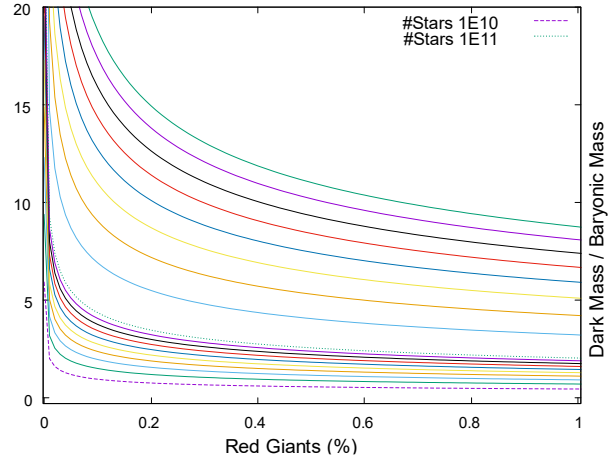

Figure 4

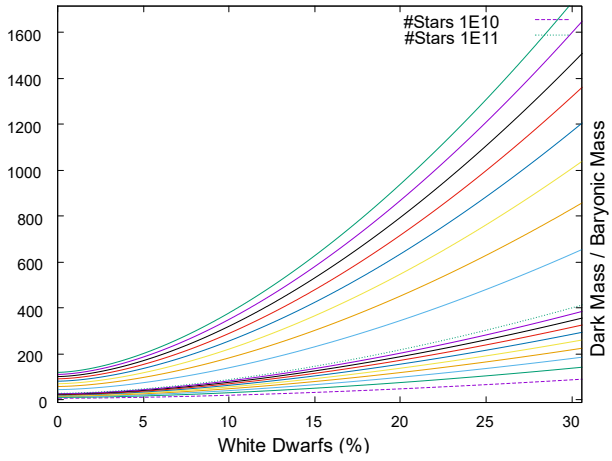

Figure 5

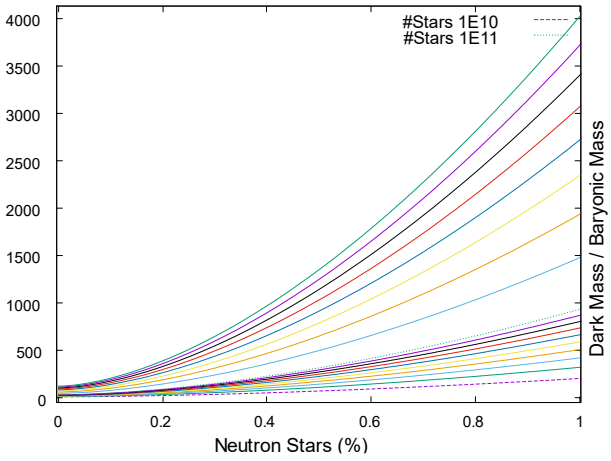

Figure 6

Black Holes

While the potential energy of stellar systems can now be calculated using the methods previously described, extending the analysis to black holes introduces additional complexity. However, the underlying principle remains the same: the gravitational potential energy is defined as the difference between two configurations—the initial, merged black hole and the final state consisting of two separate black holes.

As in the stellar case, the relevant quantity is the energy released during merger. According to general relativity (see references (15; 16)), the final mass M_f of the remnant black hole is given by:

$$M_f = (M + m)\big(1 - \eta\, \varepsilon_{\text{rad}}(q, \chi)\big)$$

where:

$$\eta = \frac{Mm}{(M+m)^2}, \quad q = \frac{m}{M} \leq 1, \quad \chi = \text{spin parameter}$$

and $\varepsilon_{\text{rad}}(q, \chi)$ is an empirical function representing the efficiency of gravitational wave emission. For non-spinning black holes, a widely used approximation is:

$$\varepsilon_{\text{rad}}(q) = 0.048 \cdot \frac{(1-q)^2}{(1+q)^4}$$

The effective spin of the remnant is given by:

$$\chi_{\text{eff}} = \frac{M\chi_M + m\chi_m}{M + m}$$

If the component black holes have randomly oriented spins, the net spin of the merged object will, on average, tend toward zero, i.e. $\chi_{eff} \approx 0$.

Let $f(m, M) \mapsto M_f$ be a function representing the final mass of a black hole formed by merging two black holes of masses m and M, according to the relativistic formula described earlier.

To extend this to the merger of n black holes, we reduce the problem to the case of n identical black holes, each of mass m, so that the total initial mass is $M = nm$. Define a recursive function $g(n, m) \mapsto M_f$ where $g(n, m)$ returns the final mass after all n black holes of mass m are merged. The function proceeds as follows:

$g(n, m) \mapsto M_f$:

IF $n = 2$ **THEN** $M_f = f(m, m)$
IF $n = 3$ **THEN** $M_f = f(m, m)$, $M_f = f(m, M_f)$,
ELSE
isOdd = *false*
IF Odd(n) **THEN** $n = n - 1$, is*Odd* = *true*
$M_f = g(n/2, m)$
$M_f = f(M_f, M_f)$
IF is*Odd* **THEN** $M_f = f(m, M_f)$

This recursive structure is well-suited for dynamic programming. By storing intermediate results of $g(a,b)$ in a memoization table, the overall number of distinct computations is reduced significantly, achieving logarithmic efficiency in the number of mergers, i.e. $O(\log_2 n)$.

Negligible Potential Energy Contribution from Black Hole Mergers

The gravitational potential energy produced by black hole mergers is extremely limited, as it is drawn directly from the initial mass of the black holes. By definition, the radiated energy—primarily in the form of gravitational waves—can never exceed the total mass-energy of the system.

Even under ideal conditions, such as an aligned prograde spin configuration (which maximizes radiative efficiency), the fraction of mass converted into gravitational wave energy remains low. Using a semi-analytical approximation derived from numerical simulations (17; 18), the radiated energy fraction is given by:

$$\frac{E_{\mathrm{gw}}}{M} \approx \eta(1-4\eta)[1-0.0686(1-\chi_{\mathrm{eff}})^2]$$

where $\eta = \frac{Mm}{(M+m)^2}$ is the symmetric mass ratio, and χ_{eff} is the effective dimensionless spin.

In the most favorable scenario—mergers involving black holes exceeding 500 solar masses and spins near unity—the maximum energy fraction remains below 16%.

Given both this upper bound and the relatively low abundance of black holes in most galactic environments, their contribution by fusion to the total gravitational potential energy of celestial systems is negligible.

Black Holes and the Problem of Volume Conservation

Despite their relatively small contribution to gravitational wave energy, it is impossible to exclude black holes from the calculation of gravitational potential energy. According to Newtonian gravity, any massive object—including black holes—contributes to the total potential energy via the standard expression $E_p = -GmM / d$.

Consider the construction of the initial compact configuration, which conserves the total volume of gas and stars and results in a body of mass M and volume V. If the system also contains n black holes of mass m and individual volume v, then—by analogy—they should be included in the compact configuration as well, leading to a revised mass and volume: $M' = M + nm$, $V' = V + nv$.

However, this treatment presents a paradox. If black holes are introduced into the compact configuration, they would, under gravitational attraction, eventually coalesce. But unlike normal matter, *the merger of black holes reduces their total volume*—a property not shared by stars. Thus, treating them analogously within a volume-conserving framework breaks the model's fundamental assumption of conservation.

This highlights a unique property of black holes, they violate volume conservation through merger. Their inclusion in gravitational potential energy calculations is necessary, but their geometric behavior introduces a conceptual inconsistency that challenges the volume-conserving assumption used to construct the compact configuration.

Black Holes and the Limiting Case of Gravitational Potential Energy

This analysis suggests that black holes must be treated analogously to ordinary matter within the volume-conserving compact configuration—but with the important caveat that their unique volume behavior under merger must be respected. In this framework, we merge all black holes present in the system into a single equivalent black hole.

The resulting object may be highly dense (e.g., density ≈ 1000 for a mass of $4.3 \times 10^6\ M_\odot$) or extremely diffuse on a geometric scale (e.g., density ≈ 0.001 for a mass of $4.3 \times 10^9\ M_\odot$) due to the non-linear scaling of Schwarzschild radius with mass. Paradoxically, the presence of a larger number of black holes—when merged into a single object—can decrease the total gravitational potential energy of the system.

This outcome is unavoidable**.** As the number and total mass of black holes increase, the system approaches the physical limit of forming a single, final black hole. According to the no-hair theorem, such a black hole has no internal structure—no mass distribution, no gravitational self-interaction, and thus no gravitational potential energy in the classical sense. It is entirely defined by its mass, spin, and charge. Consequently, black holes represent the endpoint of gravitational compaction, beyond which no further gravitational binding energy can be extracted. As their dominance in a system grows, the accessible gravitational potential energy inevitably declines.

Model Results with Varying Black Hole Fractions

Figures 7 through 10 present the results of our theoretical model for galaxies containing the same number of stars as previously considered, now fixed to solar mass and radius 1 $M_{\odot}$, 1 $R_{\odot}$. The x-axis shows the fraction of the total stellar mass that is assigned to black holes, expressed as a percentage.

At a black hole mass fraction of approximately 1.3%, the dark mass ratios for galaxies with 100, 200, and 300 billion stars converge to values of 19.7, 22, and 23, respectively. These results align well with observational constraints—particularly the commonly cited 95% dark matter proportion for the Milky Way, which corresponds to a dark mass ratio of ~20, and estimates placing the stellar mass fraction in black holes at around 1% (19).

The trend of decreasing dark mass production with increasing black hole proportion persists up to galaxy sizes of approximately one billion stars, beyond which the effect begins to reverse slightly. Remarkably, with only a 5% black hole mass fraction, most galaxies become indistinguishable from one another in terms of their dark mass ratio. At this point, only the smallest galaxies remain distinct, while larger systems converge toward a universal behavior in dark mass production.

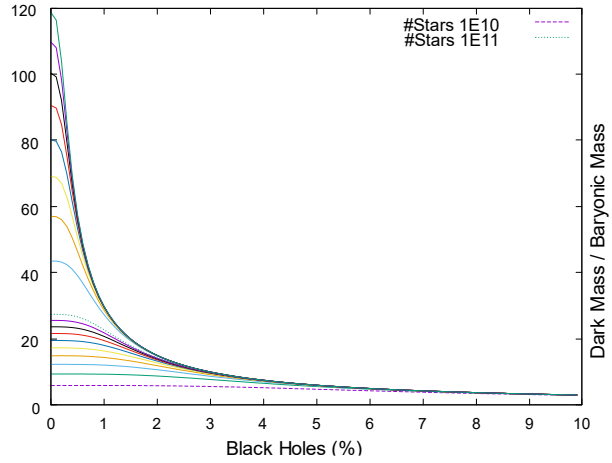

Figure 7

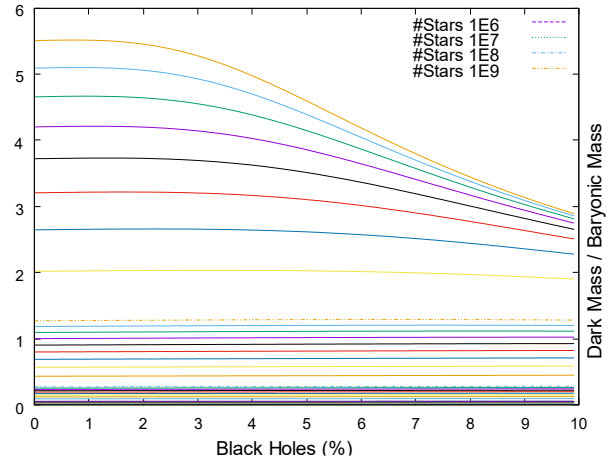

Figure 8

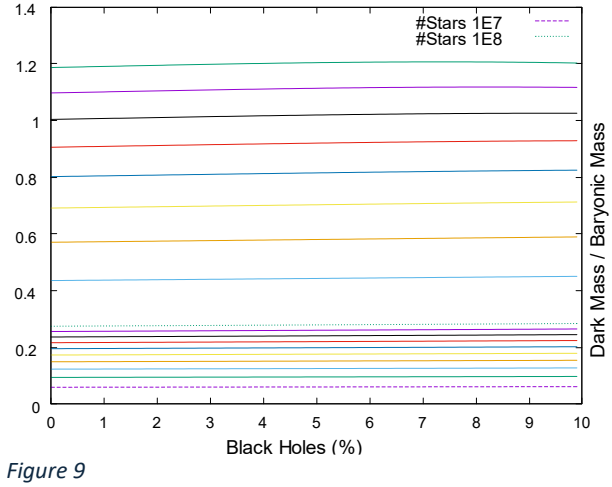

Figure 9

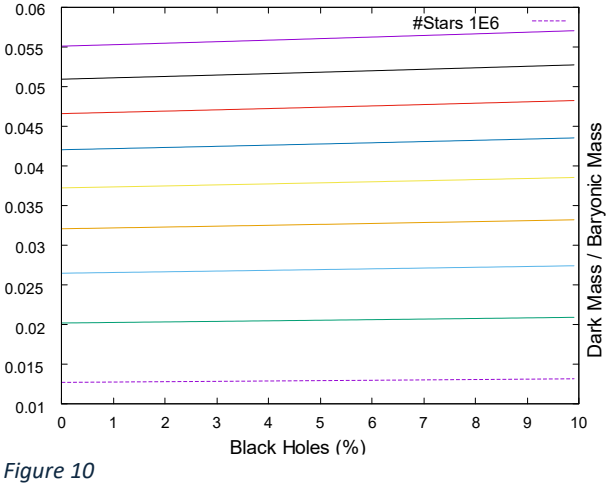

Figure 10

Galactic Models

To evaluate whether gravitational potential energy alone can account for the observed dark mass in galaxies, we tested our theoretical model against the SPARC sample (20), which includes rotation curve data for 175 galaxies along with their mass models.

For each data point, the dataset provides the observed velocity V_{obs} and the contribution of the baryonic mass contained in the orbital radius V_{bar} as well as its division in bulge stars V_{bul}, disk stars V_{disk} and gas V_{gas}. These values are used to estimate the mass contained in the orbital radius M_{bul}, M_{disk}, M_{gas} using the mass models. Subsequently, the required dark mass M_{dark} is calculated by comparing the observed acceleration to that predicted by visible matter. Each point also includes an estimate of the uncertainty eM_{dark} for the inferred dark mass.

Two galaxies (UGC 4305 and UGC 6628) were excluded due to negative global dark mass, leaving a final sample of 173 galaxies. This dataset contains 3,362 kinematic data points, of which 3,039 (approximately 90%) were retained for analysis. Data points with negative dark mass values or negative errors were removed to ensure consistency and reliability.

Stellar Population Fitting Method

For each data point in the SPARC sample, we apply our model to determine the optimal composition of stellar remnants and evolved stars—specifically black holes, white dwarfs (0.6 $M_\odot$, 0.0085 $R_\odot$), red dwarfs (0.4 $M_\odot$, 0.5 $R_\odot$), and red giants (4 $M_\odot$, 100 $R_\odot$)—that can reproduce the required dark mass M_{dark} as closely as possible. This is a simple exhaustive search (brute-force search) retaining the solution minimizing the error.

For each configuration, we compute the gravitational potential energy E_{dark} predicted by the model and evaluate the absolute deviation $\Delta_{\text{dark}} = |E_{dark} - M_{dark}|$

The fitting process aims first to bring Δ_{dark} within the observational uncertainty $\Delta_{\text{dark}} < eM_{dark}$ or $\Delta_{\text{dark}} < 2eM_{dark}$

While a more precise approach would account for both the uncertainty in the observed dark mass M_{dark} and the uncertainty in the model prediction E_{dark}, we treat eM_{dark} as the effective error margin for E_{dark} as a practical simplification.

If no composition satisfies this criterion, we minimize Δ_{dark} as a second step. Each data point is treated independently.

Model Fit Results

The model demonstrates excellent agreement with observational data. Among the 173 galaxies analyzed, 86% (149 galaxies) exhibit no residual errors across all included data points when evaluated using the relaxed threshold $\Delta_{\text{dark}} < 2eM_{dark}$. This corresponds to 81% of the total data points (2,467 out of 3,039) meeting the same condition.

Under the stricter criterion $\Delta_{\text{dark}} < eM_{dark}$, 74% of galaxies (128 out of 173) are fully resolved with no individual data point exceeding the error threshold, accounting for 71% of the retained data points.

Overall, 95% of all individual data points meet the $2eM_{dark}$ condition, and 92% fall within the stricter $1eM_{dark}$ threshold. These results confirm the robustness of the model in reproducing observed dark mass distributions across a wide range of galaxy types.

Moreover, when examining the positioning of the predicted value E_{dark} within the error bar of M_{dark} —where 0% corresponds to an exact match and 100% lies at the edge of the error bar—the results are highly concentrated near the center. For the 86% of galaxies that satisfy $\Delta_{\text{dark}} < 2eM_{dark}$, the average offset is 3% ± 9%. For the 74% of galaxies with $\Delta_{\text{dark}} < eM_{dark}$, the offset improves to 1.4% ± 1.6%.

All error margins (± e) in this analysis correspond to one standard deviation.

Population Composition in Successful Fits

One of the most compelling outcomes of the model is the physical plausibility of the stellar compositions required to reproduce the observed dark mass. For the 86% of galaxies where the model fit satisfies $\Delta_{\text{dark}} < 2eM_{dark}$, the algorithm converges to the following average stellar population composition (expressed as a fraction of the total baryonic mass):

Black holes	$5.4\% \pm 4.6\%$
White dwarfs	$30\% \pm 7.7\%$
Red giants	$20\% \pm 6.7\%$
Red dwarfs	$45\% \pm 7.7\%$

These proportions remain consistent across galaxies meeting the stricter criterion $\Delta_{dark} < eM_{dark}$, as well as those with slightly larger residuals. This consistency supports the conclusion that gravitational potential energy can account for the observed dark mass using realistic distributions of stellar types.

The relatively high fraction of white dwarfs inferred by the algorithm might be moderated by including a small proportion of neutron stars, which offer high density at lower mass. Similarly, the contribution from red giants may be partially substituted by rarer but very low density and more massive hypergiants. These adjustments would preserve the energetic balance while remaining astrophysically plausible.

Intra-Galactic Consistency and Stellar Distribution Profiles

The previous model demonstrates that it is possible to reproduce the observed dark mass entirely through gravitational potential energy generated by common stellar populations—namely black holes, white dwarfs, red dwarfs, and red giants. However, this approach optimizes each data point independently and does not enforce consistency across points within the same galaxy.

To introduce intragalactic coherence, we compute m_{bul}, m_{disk}, m_{gas} and m_{dark} , which represent the masses enclosed within the orbital slice corresponding to each data point. The proportions of stellar types and black holes assigned to a given point can only depend on the total local baryonic mass, defined as $m_{bul} + m_{disk} + m_{gas}$.

This constraint reduces the available degrees of freedom, making the fitting process more complex, but it ensures global physical consistency across the galaxy.

This is the same brute force search algorithm as before; all combinations are examined for each point and only the best one is retained.

Under this constraint, the model achieves successful fits—with no residual errors—within $\Delta_{dark} < 2eM_{dark}$ for 62% of the galaxies (108 out of 173), covering 49% of the total data points. While this represents a reduction compared to the unconstrained model, it provides a key physical advantage it enables the generation of internally consistent stellar composition profiles for each galaxy.

Figures 11 and 12 present two example galaxies illustrating the recovered stellar distribution across orbital radii, as predicted by this constrained optimization.

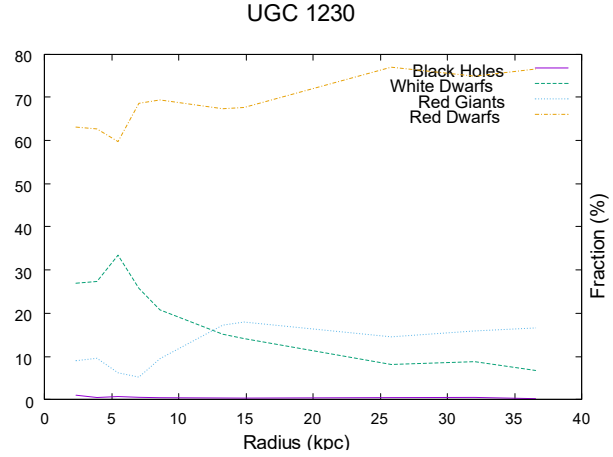

Figure 11

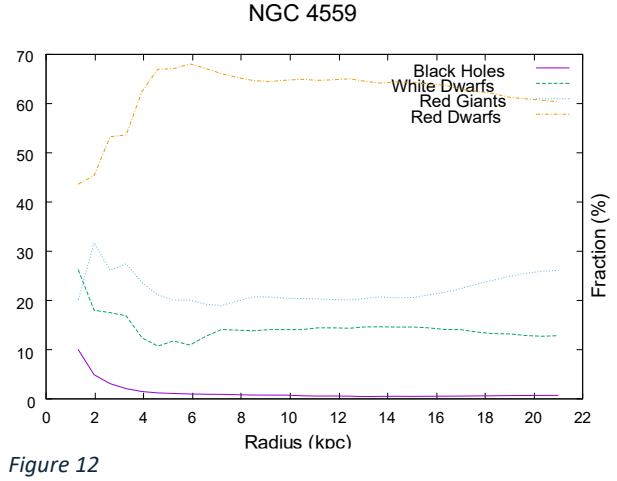

Figure 12

The Mass Energy Field

To understand how gravitational potential energy—interpreted here as dark mass—affects galactic rotation curves, we must first consider the spatial distribution of this mass-energy. Unlike baryonic matter, this invisible component is not localized in discrete particles but rather is distributed throughout the gravitational field itself.

The persistent invisibility and intangibility of this form of mass-energy presents a conceptual challenge. However, this difficulty is not entirely new. As noted by Leon Brillouin (21; 22):

"All energy has mass, but it seems that the case of potential energy has been omitted. The founders of Relativity hardly mention it. In fact, the corresponding energy is spread throughout space, and its mass cannot be exactly localized. The symmetry of the distribution suggests dividing the mass between the various interacting particles. It is therefore necessary, from classical Relativity onwards, to revise the values of the masses. Well before quanta, *renormalization* was essential (and was omitted) in Einstein's Relativity."

Brillouin's insight underscores a key theoretical omission in classical relativity, the mass-equivalence of potential energy is spatially distributed and cannot be attributed to any single point. This aligns with our interpretation, the gravitational potential energy of a system manifests as an extended, nonlocal mass-energy field. As such, the field itself contributes to the curvature of spacetime, producing the dynamical effects attributed to dark mass.

Field Proportionality and the Localization of Dark Mass

Although the problem of the mass associated with gravitational potential energy was clearly articulated by Brillouin in 1965, it has not received a satisfactory treatment in either classical or relativistic physics. In this work, we postulate that the mass stored in the gravitational field is directly proportional to the intensity of the field at a given point.

Let $\Phi(E_a)$ denote the gravitational field produced by a dark mass E_a at position a, and $\Phi(M_a)$ the field produced by a baryonic mass M_a at the same point. Likewise, at position b, let $\Phi(M_b)$ and $\Phi(E_b)$ denote the baryonic and dark field components, respectively. We assume the following proportionality relationship:

$$\frac{\Phi(E_b)}{\Phi(E_a)} = \frac{\Phi(M_b)}{\Phi(M_a)}$$

Using the standard expression for the gravitational field produced by a point mass,

$$\Phi(M) \propto \frac{M}{R}$$

where R is the characteristic radius or distance from the source, we obtain:

$$\frac{\Phi(M_b)}{\Phi(M_a)} = \frac{M_b R_a}{M_a R_b} \quad \text{and} \quad \frac{\Phi(E_b)}{\Phi(E_a)} = \frac{E_b R_a}{E_a R_b}$$

Equating the two ratios leads to:

$$\frac{E_b R_a}{E_a R_b} = \frac{M_b R_a}{M_a R_b}$$

which simplifies to:

$$\frac{E_b}{E_a} = \frac{M_b}{M_a} \quad \Rightarrow \quad E_b = E_a \cdot \frac{M_b}{M_a}$$

This relation provides a simple but powerful rule, the local dark mass is proportional to the local baryonic mass, under the assumption that gravitational field strength governs the distribution of field-stored mass-energy.

Component Contributions to Dark Mass Production

In the galactic context, the production of gravitationally induced dark mass must be analyzed component by component, as each baryonic contributor exhibits a different efficiency in generating potential energy. In practice, the available observational data typically separate the baryonic mass into at least two components, the gas mass and the stellar disk mass.

If the gas component contributes a dark mass E_{gas} from a baryonic mass M_{gas} at point a, and the stellar disk contributes E_{disk} from a baryonic mass M_{disk} at point a, it is necessary to compute their relative contributions to the total gravitationally induced dark mass at point b. These can be expressed as:

$$e_{\text{gas}} = \frac{E_{\text{gas}}\, m_{\text{gas}}}{M_{\text{gas}}}, \quad e_{\text{disk}} = \frac{E_{\text{disk}}\, m_{\text{disk}}}{M_{\text{disk}}}$$

The total contribution at point b is then $e_{\text{tot}} = e_{\text{gas}} + e_{\text{disk}}$

However, this division is still simplistic. As shown earlier, the gravitational potential energy varies significantly depending on stellar type (e.g., red dwarfs, red giants, white dwarfs, black holes). A more accurate treatment would require dividing the baryonic mass into multiple categories, each with distinct mass and radius parameters. These variations determine the gravitational binding energy and thus the amount of dark mass effectively "generated" by each category. A coarse two-component model can serve as an approximation, but more detailed modeling is essential for precision.

Two-Component Model with a Single Fitting Parameter

In the absence of detailed information about stellar sub-populations, we restrict the analysis to the two primary baryonic components typically available in observational data, gas and the stellar disk. Their respective contributions to the gravitationally induced dark mass are modeled using a single free parameter f, which represents the fraction of E_{dark} attributed to the gas component.

The total modeled dark mass is expressed as:

$$E_{\text{dark}} = E_{\text{gas}} + E_{\text{disk}} = fE_{\text{dark}} + (1-f)E_{\text{dark}}$$

From this, we define the relative contributions for each data point as:

$$e_{\text{gas}} = \frac{fE_{\text{dark}}\, m_{\text{gas}}}{M_{\text{gas}}}, \quad e_{\text{disk}} = \frac{(1-f)E_{\text{dark}}\, m_{\text{disk}}}{M_{\text{disk}}}$$

where:

- E_{dark} , M_{gas}, and M_{disk} are values measured at the midpoint radius of the galaxy.
- e_{dark}, m_{gas} and m_{disk} are values measured at the data point.

The parameter f is optimized once per galaxy and applied uniformly across all data points. Despite its simplicity, this model reproduces the observed dark mass within the margin of error for 76 of the 175 galaxies in the SPARC sample—corresponding to 43% of the dataset.

To remain conservative in our error analysis, we assign to each calculated value e_{tot} the same uncertainty as that of the corresponding observed dark mass e_{dark}.

Figures 13 and 14 illustrate representative examples of galaxies well fitted by this single-parameter, two-component model.

Incremental Refinement of the Two-Component Model

It is possible to increase the accuracy of the model by introducing additional f parameters, each associated with a distinct radial region of the galaxy. These parameters allow the relative weighting between gas and stellar disk contributions to vary spatially, thereby improving the fit to the observed dark mass profile.

For each segment, the scaling is performed using the midpoint of the segment as the local reference, with its own values of E_{dark} , M_{gas}, and M_{disk}. This ensures that the proportional calculation within each region remains physically consistent and properly normalized.

Using two *f* parameters, we achieve error-free fits for 29 additional galaxies. Allowing three *f* parameters yields an additional 6 galaxies with perfect fits. In total, this approach provides error-free solutions for 111 out of 175 galaxies, or approximately 63% of the SPARC sample.

The ability to reproduce the observed dark mass distributions across such a large fraction of galaxies—using only local baryonic mass and gravitational potential energy scaling—strongly supports the existence of a direct, physically meaningful relationship between baryonic mass and the inferred dark mass. This reinforces the core hypothesis that gravitational potential energy, when correctly modeled, accounts for the so-called dark matter without requiring matter.

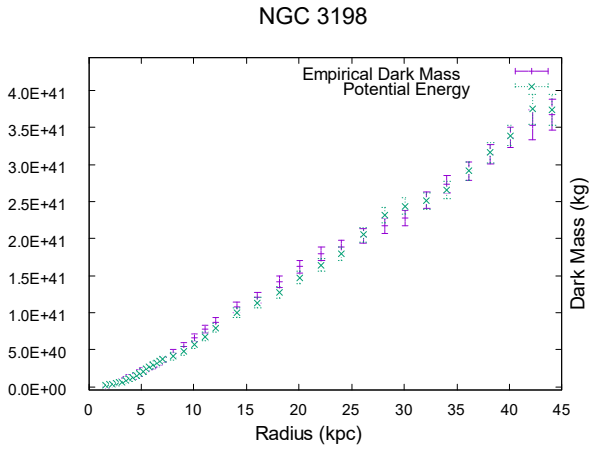

Figure 13

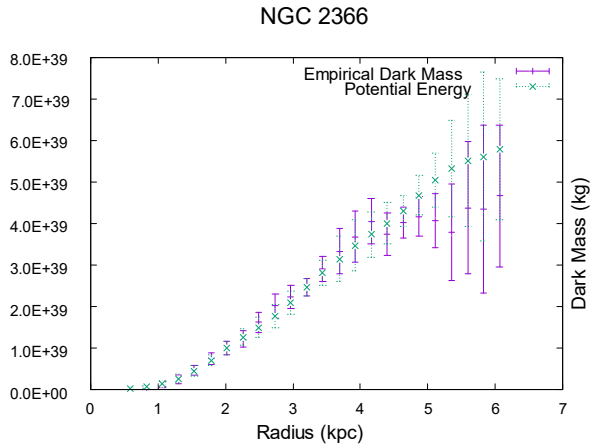

Figure 14

Dark Energy

In previous models for calculating the gravitational potential energy of self-gravitating systems (galaxies, clusters, etc.), the large-scale direct interaction term between distant bodies was considered negligible (see the section "the potential energy of celestial systems"). This term, of the form $-GmM / d$, where *d* can be interpreted as the mean separation between bodies, is indeed extremely small on stellar scales. However, at cosmological scales, and when summed over all bodies in the universe, its contribution becomes significant.

Let us consider a set of *n* point masses of mass *m*, separated on average by a distance *d*, for a total mass $M = nm$. The sum of interactions between each mass and the cumulative preceding ones yields a potential energy:

$$\Delta E_i = \frac{-GmM_i}{d}, \Delta E_{dil} = \sum_{i=1}^{n-1} \Delta E_i = -\frac{Gm^2}{d} \sum_{i=1}^{n-1} i = -\frac{Gm^2}{d} \cdot \frac{n(n-1)}{2} \approx -\frac{GM^2}{2d} \quad (\text{for } n \gg 1)$$

This energy describes the "diluted" state of the universe, a configuration of weakly bound masses at large distances.

Gravitational Compaction Energy

In contrast, if the same total mass *M* is compacted into a homogeneous solid sphere of radius *R* (e.g., preserving solar density), the gravitational potential energy becomes:

$$\Delta E_{\text{comp}} = -\frac{3GM^2}{5R}$$

The energy difference between these two configurations is:

$$\Delta E_p = \Delta E_{\text{dil}} - \Delta E_{\text{comp}} = GM^2 \left(\frac{3}{5R} - \frac{1}{2d}\right)$$

This expression is always positive for $R \ll 2d$, which is indeed the case in the real universe, $R \sim 10^{16}$ m (solar density), $d \sim 10^{26}$ m (average intergalactic separation or corrected Hubble radius), $R/d \sim 10^{-10}$, making the effective contribution significant.

A crucial observation is that R is fixed (set by the compactness and chosen density), while d increases with cosmic expansion. Therefore, the effective gravitational potential energy ΔE_p increases with d (and thus with volume V):

$$\frac{d\Delta E_p}{dV} > 0 \quad \Rightarrow \quad P = -\frac{d\Delta E_p}{dV} < 0$$

This result is interpreted as a negative gravitational pressure, not originating from an exotic scalar field, but from the geometric evolution of a structured gravitational field. As space expands, background gravitational interactions weaken, leading to a growing potential energy. Its negative derivative acts as a repulsive pressure — a natural source of accelerated expansion.

Application to the Observable Universe at Galactic Density

Instead of compacting the total mass of the universe to stellar density (e.g., the Sun), we assume here that cosmic matter is structured in the form of galactic halos containing both baryonic and dark matter. These halos are modeled as oblate ellipsoids with a horizontal radius R_{halo} and a vertical height $h = \alpha R_{\text{halo}}$, where α is a shape factor.

The average volume of a galactic halo is then written as:

$$V_{\text{gal}} = \frac{4}{3}\pi R_{\text{halo}}^2 \cdot \alpha R_{\text{halo}} = \frac{4}{3}\pi\alpha R_{\text{halo}}^3$$

The average density of a galactic halo, including both baryonic and dark matter, is given by:

$$\sigma_{\text{gal}} = \frac{M_{\text{gal}}}{V_{\text{gal}}} = \frac{3M_{\text{gal}}}{4\pi\alpha R_{\text{halo}}^3}$$

Assuming the universe consists of N identical galaxies, each of mass M_{gal}, the total mass is:

$$M_{\text{tot}} = NM_{\text{gal}}$$

and the total equivalent volume becomes:

$$V_n = NV_{\text{gal}} = \frac{M_{\text{tot}}}{\sigma_{\text{gal}}}$$

This volume is equal to that of a compact sphere of radius R, such that:

$$\frac{4}{3}\pi R^3 = \frac{M_{\text{tot}}}{\sigma_{\text{gal}}} \quad \Rightarrow \quad R_n = \left(\frac{3}{4\pi} \cdot \frac{M_{\text{tot}}}{\sigma_{\text{gal}}}\right)^{1/3}$$

This result is important, it shows that regardless of the geometric shape of the halos, the effective radius R depends solely on the average galactic density σ_{gal}. The geometric factor α cancels out entirely, providing this modeling with remarkable robustness.

By compacting the total mass of the observable universe $M_{\text{tot}} \approx 8.8 \times 10^{52}$ kg compatible with ΛCDM) to a galactic density compatible with the SPARC, EAGLE, and Illustris samples, $\sigma_{\text{gal}} \in [3.0 \times 10^{-22}, 2.0 \times 10^{-21}]$ kg/m^3 we obtain an effective radius $R \in [2.2 \times 10^{24}, 4.1 \times 10^{24}]$ m.

The gravitational potential energy of such a structured system is given by:

$$\Delta E_p = GM_{\text{tot}}^2\left(\frac{3}{5R} - \frac{1}{2d}\right)$$

Using $d = kc/H \approx 4.5 \times 10^{26}$ m with $k = 3.27$ which is the comoving factor associated with the Hubble radius in ΛCDM, the numerical evaluation leads to $\Delta E_p \in [7.5 \times 10^{70}, 1.4 \times 10^{71}]$ J. What falls within the current estimate of the observable universe $\Delta E_\Lambda \in [6.6 \times 10^{70}, 2.6 \times 10^{71}]$ J (Planck 2018, WMAP, SNIa, BAO).

Our equation can be rewritten in such a way as to deduce the total mass M_{tot} by a dependence on the ratio Ω_Λ/Ω_m, the error of which is better understood, as well as on the galactic density by R_n and on the Hubble radius by d.

$$M_{\text{tot}} = \frac{c^2}{G} \cdot \frac{\Omega_\Lambda}{\Omega_m} \cdot \left(\frac{3}{5R} - \frac{1}{2d}\right)^{-1}$$

We can use the usual cosmological constants and a comoving radius of $d \approx 4.5 \times 10^{26}$ m, a dark energy to matter ratio $\Omega_\Lambda/\Omega_m \approx 2.17$ and a galactic density of $\sigma_{gal} \approx 1.2 \times 10^{-21}$ kg/m^3 producing a compact effective radius $R \approx 2.6 \times 10^{24}$ m, to calculate the mass M_{tot} (baryonic + galactic dark mass). Since R depends on M_{tot}, we must find M_{tot} generating R stabilizing its own value, that is $M_{\text{tot}} \approx 4.81 \times 10^{51}$ kg producing $\Delta E_p \approx 9.38 \times 10^{68}$ J of dark energy. Which is too little and does not respect ΛCDM.

To summarize, if we consider that the mass of the Universe $M_{\text{tot}} \approx 8.8 \times 10^{52}$ kg is found entirely in galaxies then it is possible to produce the potential energy respecting the dark energy. However, our equation allows us to calculate exactly the total galactic mass, and it is only $M_{\text{tot}} \approx 4.81 \times 10^{51}$ kg or almost twenty times less.

This is perfectly understandable because if dark energy is indeed diffuse gravitational potential energy, the ratio $\Omega_\Lambda/\Omega_m \approx 2.17$ is a misinterpretation. It overestimates the "cosmological constant" by ignoring the dynamical contribution of structuring. A significant part of the gravitational effect attributed to Ω_m should be accounted for in Ω_Λ. The ΛCDM model then underestimates the energetic contribution of the structured field (i.e., Ω_Λ), while overestimating the matter density. This implies a possible revision of the Ω_Λ/Ω_m ratio, suggesting that the universe contains more diffuse dark mass (dark energy) than previously thought.

While the term $1/2d$ is less important (< 1%) in the calculation of the total gravitational potential energy—dominated by the compact term $3/5R$—it plays a crucial role in the dynamics of cosmic expansion. What is commonly referred to as dark energy is, in fact, the gravitational potential energy associated with the large-scale distribution; that is, the global dark mass. However, it is not the magnitude of this energy that drives accelerated expansion, but the variation of the $1/2d$ term with cosmic volume. As the universe expands and d increases, the gravitational dilution term decreases, producing an effective negative pressure. This evolving contribution, although small in absolute energy, could be the real driving force behind the repulsive effect attributed to dark energy in the ΛCDM cosmology.

Emergent Pressure from Gravitational Potential

The effective gravitational potential energy of the structured system, previously written as:

$$\Delta E_p = GM^2 \left(\frac{3}{5R} - \frac{1}{2d}\right)$$

can be expressed as a function of cosmic volume V, noting that R, is constant (galactic structure is assumed stable), $d = (3/4\pi)^{1/3} V^{1/3}$ then:

$$\Delta E_p(V) = GM^2 \left(\frac{3}{5R} - \frac{1}{2(3/4\pi)^{1/3} V^{1/3}}\right)$$

The corresponding effective pressure is:

$$P(V) = -\frac{d\Delta E_p}{dV} = -GM^2 \cdot \frac{1}{2(3/4\pi)^{1/3}} \cdot \frac{1}{3} V^{-4/3} = -\frac{GM^2}{6(3/4\pi)^{1/3} V^{4/3}}$$

This pressure is strictly negative and decreases with expansion. It does not stem from exotic substances or hypothetical fields but arises from the weakening of gravitational interaction as volume increases. This macroscopic potential energy, generated by gravitational structuring, stores information in the field itself. Its derivative manifests as a repulsive effect — a geometric mechanism that can mimic dark energy.

Integration into General Relativity

In general relativity, the source of spacetime curvature is not mass alone, but the energy–momentum tensor $T_{\mu\nu}$. For a homogeneous and isotropic universe, this tensor reduces to that of a perfect fluid:

$$T^{\mu\nu} = \left(\rho + \frac{P}{c^2}\right) u^\mu u^\nu + P g^{\mu\nu}$$

The pressure obtained above is not a hypothesis but a geometric consequence of the gravitational field's structure. It is thus natural to consider this pressure — arising from effective potential energy — as contributing to a gravitational component of the energy–momentum tensor:

$$T_{\text{grav}}^{\mu\nu} = \left(\rho_{\text{pot}} + \frac{P_{\text{grav}}}{c^2}\right) u^\mu u^\nu + P_{\text{grav}} g^{\mu\nu}$$

where:

$$\rho_{\text{pot}} = \frac{\Delta E_p}{V}, \quad P_{\text{grav}} = -\frac{GM^2}{6(3/4\pi)^{1/3} V^{4/3}}$$

This tensor has the same structure as that of dark energy, but its origin is not constant — it emerges dynamically from the gravitational structuring of the universe. So, the complete equation is:

$$G_{\mu\nu} = \frac{8\pi G}{c^4}\left(T_{\mu\nu}^{\text{matter}} + T_{\mu\nu}^{\text{grav}} + T_{\mu\nu}^{\Lambda}\right)$$

Reproducing ΛCDM Cosmology

To assess the cosmological implications of this effective pressure, we substitute it into the Friedmann equations. Assuming a spatially flat universe ($k = 0$):

$$\frac{\ddot{a}}{a} = -\frac{4\pi G}{3}\left(\rho + \frac{3P}{c^2}\right)$$

With:

$$\rho = \frac{M}{V}, \quad P = -\frac{GM^2}{6(3/4\pi)^{1/3} V^{4/3}}$$

We obtain the dynamical equation for cosmic volume:

$$\frac{\ddot{V}}{V} = -\frac{A}{V} + \frac{B}{V^{4/3}} + \frac{1}{3}\left(\frac{\dot{V}}{V}\right)^2 + \Lambda V$$

with $A \propto GM$ and $B \propto G^2M^2 / c^2$ and the last term ΛV representing dark energy in the form of a cosmological constant.

Dimensionless Transformation

The previous differential equation is not directly soluble numerically due to the extreme scales involved. We therefore introduce dimensionless quantities:

- $V \rightarrow V/V0$, where $V0$ is the current volume of the universe,
- $t \rightarrow \tau = t/t_0$ where t_0 is the current age of the universe.

This implies a change of scale for the time derivatives, for example:

$$\frac{dV}{dt} \rightarrow \frac{V_0}{t_0}\frac{dV}{d\tau}, \quad \frac{d^2V}{dt^2} \rightarrow \frac{V_0}{t_0^2}\frac{d^2V}{d\tau^2}$$

and the constants become:

$$\tilde{A} = \frac{GMt_0^2}{V_0}, \quad \tilde{B} = \text{FP} \cdot \tilde{A}, \quad \tilde{\Lambda} = \Lambda t_0^2$$

where *FP* is a free parameter representing the intensity of the effective pressure. We also allow a generalization of the exponent 4/3 by introducing a multiplicative factor *FE*, which acts on the effective definition of the mean radius and allows us to explore cases of anisotropy or internal structure.

The final dimensionless equation is written:

$$\ddot{V} = -k\tilde{A}/V + 0.5 \cdot k\tilde{B}/V^{4FE/3} + \frac{1}{3}\left(\frac{\dot{V}}{V}\right)^2 + \tilde{\Lambda}V$$

The factor $(4\pi/3)^{1/3}$ comes from spherical geometry, because the average radius in a volume V is given by $R = (3V/4\pi)^{1/3}$. It is this relationship which is at the origin of the coefficient $k = 4\pi/3$ introduced in the dimensionless version.

The Pressure Factor (*FP*)

The *FP* factor simply measures the ratio of effective pressure to gravitational attraction. In classical theory, the natural factor would imply:

$$\frac{B}{A} \sim \frac{GM}{c^2}\left(\frac{GM}{V^{1/3}}\right) \cdot \left(\frac{1}{A}\right)$$

But in a dimensionless framework, this effective constant is absorbed into *FP*. It then becomes a freely adjustable parameter, which can be positive or negative, depending on whether the effective pressure amplifies or counterbalances the overall gravitational attraction. This parameter is the most important because it modifies the position of the curve on the y axis, i.e. $q(z)$.

The Exponent Factor (*FE*)

The effective pressure depends on the mean radius of the universe, denoted *d*, related to the volume *V* by:

$$d = \left(\frac{3V}{4\pi}\right)^{1/3}$$

This definition is based on an assumption of homogeneity and spherical isotropy. It becomes less restrictive if we admit more complex internal structures, anisotropies, or effective geometries, for example in a filamentary network universe.

Moreover, the inverse relation $V = 4\pi\, d^3 / 3$ is geometrically strict but physically arbitrary if we consider that *d* is only an average of characteristic distances.

Thus, we generalize the 4/3 exponent of the pressure term by replacing it with:

$$\frac{B}{V^{4FE/3}}$$

where *FE* is a free exponent factor (by default *FE* = 1). This amounts to introducing a generalized relationship between mean radius *d* and volume *V*:

$$d \propto V^{FE/3}$$

and to consider that gravitational pressure is expressed as:

$$P \propto -\frac{1}{d^4} \propto -\frac{1}{V^{4FE/3}}$$

This *FE* parameter therefore makes it possible to modulate the geometric dependence of gravitational pressure on the structure of the universe and to finely adjust the dynamic behavior of the equation to better match the observations (particularly around the transition redshift). Concretely, it makes it possible to slightly modify the shape of the curve, particularly in the zone $z < 2$.

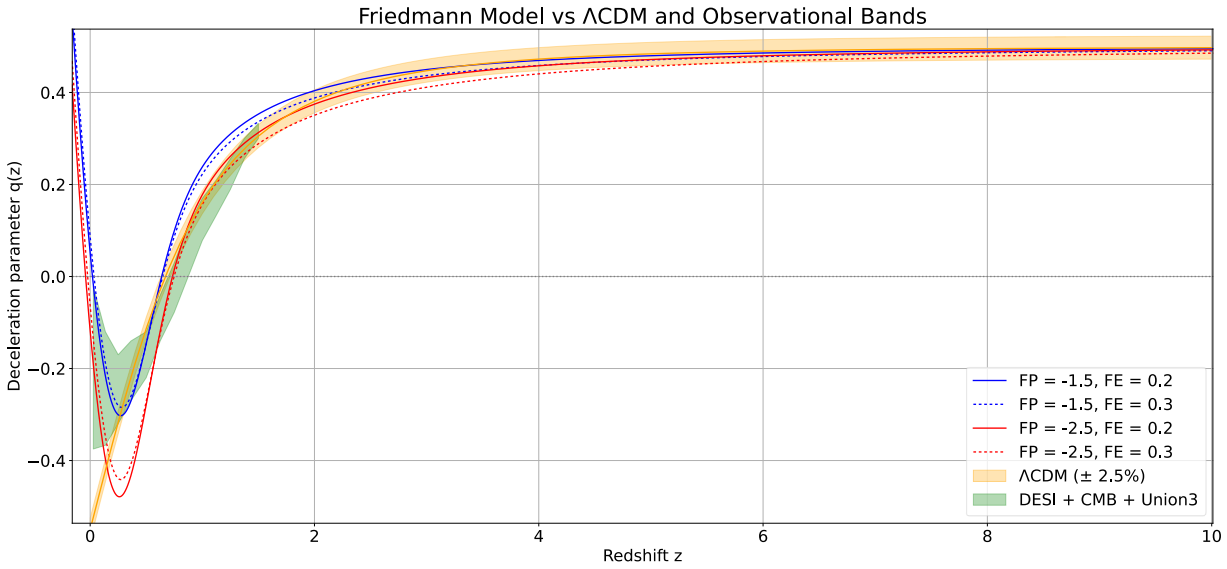

Discussion on the Setting

We see, once again, that despite the many necessary simplifications, the curve fit is excellent. However, the use of two parameters allows for a fit that leaves reasonable doubt. That said, it is important to note that the position of the inflection (for $z < 3$) is at the beginning of the curve, and that the control over the increase or decrease of the flare is practically zero. The same is true for the slope of the quasi-line (for $z > 3$), which remains stable regardless of the parameterization.

We were unable to identify a parameterization that perfectly matches current observational measurements (DESI + CMB + Union3), although we are close. However, it is easy to reproduce the ΛCDM model in the range $z = 0.6$ to $z = 10$. Moreover, although none of the generated curves exactly fit the observational data for $z < 1.5$, the four variants explored collectively cover different regions of this data space. The fact that the inflection rate depends mainly on the *FE* factor suggests that the isotropy assumption may be inaccurate, and that the calculation of the average distance requires more than a simple exponent.

The parameter dV_0, representing the initial expansion speed in the model, is not free, it depends entirely on the factor *FP*. Changing the initial volume V_0 changes absolutely nothing in the interval $z = 0$ to $z = 10$, so any translation on the redshift axis is therefore legitimate. On the other hand, we were unable to vary the cosmological constant Λ, which turned out to be much too sensitive. Finding a parameter Λ that did not cause the numerical solver to collapse proved extremely difficult. Therefore, we set $\Lambda = 0$.

Discussion on the Margin of Error

Calculation of Dark Energy

If we consider the calculation of dark energy, our function *f* projects the galactic $\sigma_{gal} \in [3.0 \times 10^{-22}, 2.0 \times 10^{-21}]$ kg/m^3 into a range of potential energy $\Delta E_p \in [7.5 \times 10^{70}, 1.4 \times 10^{71}]$ J itself contained in the interval of the measured dark energy $\Delta E_\Lambda \in [6.6 \times 10^{70}, 2.6 \times 10^{71}]$ J. This overlap could, apparently, result from chance. However, let us analyze this possibility. The probability that a significant figure such as 7.5 falls in the interval [6.6, 26] is about 19.4%, and the same is true for 14. The probability that both values are simultaneously included in this interval is therefore 19.4% × 19.4% ≈ 3.76%.

If we also consider that the exponent 10^{70} is the correct one, among a reasonable range of exponents from 40 to 100, then the probability is 1 / (100 – 40 + 1) ≈ 1.64%. The total probability that this match is the result of chance therefore becomes 3.76% × 1.64% ≈ 0.062%, which corresponds to about one chance in 1,600, a probability well below a threshold of 3σ (about 0.27%).

The presented probabilistic calculation is based on a simple but rigorous estimate of numerical chance. It relies on the fact that the value of ΔE_p, derived solely from unadjusted physical data—the total mass of the universe $M_{tot} \approx 8.8 \times 10^{52}$ kg, and the galactic density range—falls within the experimental dark energy range E_Λ, without recourse to a free fit. The Hubble constant H_0 enters this calculation with an influence of less than 1% and therefore has no significant impact on the result. The probabilistic calculation estimates the chance that this result agrees both in significant figures and in orders of magnitude. These probabilities are considered independent and combined in a standard way. This approach is justified when assessing the likelihood that such precise agreement is due to chance alone, in a setting without free fit.

Calculation of the Friedmann Model

Rigorously assessing the probability that a model-generated curve coincidentally matches a shape consistent with observations is complex. Nevertheless, some structural features of the model are remarkably stable across parameterizations. We rely on this robustness to estimate the probability that such agreement with empirical data results from chance.

First, the main inflection point around $z = 0.25$, which marks the transition from cosmological acceleration to deceleration, could just as well have been convex. In the absence of any dynamical constraint imposing the observed concavity, a priori probability of 50% can reasonably be assigned to this configuration.

Second, the passage into the zero-deceleration zone ($q(z) = 0$), located between $z = 0.6$ and $z = 0.9$, could have appeared anywhere in a wide interval, for example between $z = 1$ and $z = 11$. The probability that the curve falls precisely in the observed interval is therefore of the order of (0.9 - 0.6) / (11 - 1) = 3%.

Third, the convergence of the curve to the ΛCDM plateau at $q(z) \approx 0.4$ around $z = 1$ could never have occurred and converge to any other value of q, up to an arbitrary maximum of $q = 1.4$, which is very conservative. Considering a tolerance band of width $\Delta q = 0.1$ centered on the plateau, the probability of such an alignment is approximately 1%.

Finally, the quasi-linear portion of the curve between $z = 3$ and $z = 10$ must maintain a very narrow slope to remain within the band $q(z = 10) \in [0.472, 0.522]$. Restricting the admissible slopes to the interval $[3 \times 10^{-3}, 11 \times 10^{-3}]$, and assuming a uniform distribution of slopes to two significant figures, the probability of such accuracy is estimated to be 8%. Also considering a 10% probability that the exponent is 10^{-3}, the total probability of maintaining a compatible slope is 0.8%.

The joint probability of obtaining these four structural characteristics simultaneously by pure chance is therefore 50% × 3% × 1% × 0.8% = 1.2×10^{-6} which corresponds to a chance of about 830,000, i.e. beyond the significance threshold of 4.5σ.

The assessment of the probability that a model spontaneously reproduces the main observed characteristics relies on a series of distinct events in the evolution of the deceleration curve. Each event—such as the concavity of the inflection around $z \approx 0.25$, the passage through the zero deceleration zone $q(z) = 0$ between $z = 0.6$ and $z = 0.9$, the absence of drift towards divergent values around $z \approx 1.0$, or the stability of the slope of the quasi-line for $z > 3$—represents a condition that could have not been satisfied. These behaviors are structurally independent in the dynamics of the model; the realization of one does not mechanically constrain the others. Their simultaneous conjunction therefore becomes a highly specific combined event. The product of their probabilities constitutes, in this context, a relevant approximation of the overall likelihood.

Calculation of Dark Mass

The possibility of obtaining the total dark mass by combining different stellar populations is based, by analogy, on the resolution of a system of the type:

$$m_1 x_1 + m_2 x_2 + m_3 x_3 + m_4 x_4 = M, \quad x_1 + x_2 + x_3 + x_4 = 1, \quad 0 \leq x_i \leq 1$$

In the linear case, it is known that about 60% of systems admit a solution in the hypercube $[0,1]^4$ (tesseract) for random m_i coefficients. However, the system modeling our energy composition is strongly nonlinear, constrained by additional physical properties. Despite this, the obtained numerical results not only satisfy the imposed constraints but produce compositions consistent with astrophysical observations.

Our function f simply maps, for each data point, a baryon mass M_{bar} and a galactic composition C_{gal} to the estimated dark mass M_{dark}, that is, $E_{cal} = |M_{dark} - f(M_{bar}, C_{gal})|$, which we compare to the experimental error eM_{dark}. We consider the point resolved if there exists C_{gal} such that $E_{cal} < 2eM_{dark}$ and unresolved otherwise. The assumption that every (M_{bar}, M_{dark}) combination can be resolved by a C_{gal} combination seems false, because we fail to do so. However, under this assumption, there should be no difference in the resolving power of a (M_{bar}, M_{dark}) and (M_{bar}, τM_{dark}) point, where τ is a reasonable fraction (90% to 30% or 111% to 333%). Thus, our algorithm should not differentiate between a real experimental point and a random variation of it.

So we will construct random variations of our galactic sample (SPARC) by multiplying the dark mass of all galaxy data points by a random factor τ (one factor τ per galaxy). We will solve one hundred (100) modified galaxy sets and compare their results to the original set. We will use intervals of the type $\tau \in$ [min%, max%] or $\tau \in$ [1/max%, 1/min%] with max% – min% = 10%. This ensures that we have both comparable dark mass decreases and increases. We used a constant relative error and so the error is τeM_{dark}, using the absolute error does not change the results much but it is mathematically incorrect.

We will compare the proportion G_{good} of galaxies resolved without error, that is, the proportion of galaxies for which all their data points are resolved, and the proportion P_{good} of points falling within these galaxies. For our original sample without modification, we have $max(G_{good})$ = 86% and $max(P_{good})$ = 81%. We will always present the lower z-score between G_{good} and P_{good}.

For $\tau \in$ [80%, 90%] or $\tau \in$ [111%, 125%], we find $max(G_{good})$ = 87% > 86% and $max(P_{good})$ = 83% > 81% with a z-score of 0.9σ. So, this small variation simply acts as a form of bootstrapping to improve the results. Then, for $\tau \in$ [70%, 80%] or $\tau \in$ [125%, 142%], we find $max(G_{good})$ = 85.5% < 86% and $max(P_{good})$ = 81.7% > 81% with a z-score of 2.27σ. With $\tau \in$ [60%, 70%] or $\tau \in$ [142%, 166%], we have $max(G_{good})$ = 85% < 86% and $max(P_{good})$ = 81.7% > 81% with a z-score of 2.83σ. At $\tau \in$ [50%, 60%] or $\tau \in$ [166%, 200%], we have $max(G_{good})$ = 83% < 86% and $max(P_{good})$ = 79% < 81% with a z-score of 3.14σ. Then at $\tau \in$ [40%, 50%] or $\tau \in$ [200%, 250%], we have $max(G_{good})$ = 78% < 86% and $max(P_{good})$ = 72% < 81% with a z-score of 5.27σ. Finally at $\tau \in$ [30%, 40%] or $\tau \in$ [250%, 333%], we have $max(G_{good})$ = 73% < 86% and $max(P_{good})$ = 64% < 81% with a z-score of 7.33σ.

Thus, our algorithm seems to distinguish "*good*" galaxies from "*bad*" ones that have been modified, which completely contradicts the initial hypothesis. It is clear that beyond a certain threshold, no realistic composition of stars and black holes could satisfy the values. In extreme cases, only a population of black holes could satisfy the low range and white dwarfs the high range.

Considering only factors τ > 100%, our algorithm performs optimally in the region $\tau \in$ [1, 1.25] and fails beyond that, for example for $\tau \in$ [1.25, 100]. However, if this were a random event, it could have performed optimally anywhere in this range. The probability of this event is therefore 1/400. Moreover, these are in fact masses of the order of 10^{40} kg, and even remaining conservative, the probability of being in this range is less than 1/10. Then, the fact that our optimal solutions place on average the proportion of red dwarfs in first place and that of black holes in last had only a probability of 1/8 of occurring randomly. This for a total of 1/32,000 or approximately 4σ.

Final Cumulative Margin of Error

Finally, by combining all the elements studied—namely, the quantitative agreement of the dark energy calculation, the consistent shape of the deceleration curve with observations, and the energetic correspondence with the galactic dark mass—we obtain an overall probability of less than 1/1,600 × 1/830,000 × 1/32,000, which corresponds to a statistical significance level greater than 7.5σ. Therefore, even if we remain very conservative, we reach 5σ.

Conclusion

The objective of this article was to demonstrate that the phenomenon commonly referred to as “dark matter” can be fully accounted for by gravitational potential energy. Through both theoretical and empirical approaches, we have shown that the potential energy generated by gravitational interactions—particularly when applied to systems like the Earth–Moon or Earth–Sun—is far from negligible and must be considered as a real, physical quantity.

Using simplified theoretical models, we established that this potential energy, when converted via the mass–energy equivalence relation $E = mc^2$, yields contributions on the same order of magnitude as the dark mass inferred from galactic rotation curves.

We subsequently compared our theoretical model to a substantial body of observational data and obtained an excellent fit, despite the necessarily simplified assumptions used throughout. This empirical success provides a necessary condition for validating the model; the gravitational potential energy predicted by the distribution of baryonic mass must be sufficient to account for the observed dark mass. Our results show that this condition is fulfilled across a wide range of galaxy types.

We then extended our model by applying the principle of causal proportionality—namely, that identical mass distributions of the same type must generate proportionally identical effects. If a baryonic mass M, composed of stars of a given type (e.g., solar-mass stars), produces a corresponding dark mass E, then a subcomponent of mass m will generate a dark mass:

$$e = \frac{Em}{M}$$

When expressed as a gravitational field, this implies that the spatial distribution of dark mass follows the distribution of baryonic mass—provided that the composition (stellar types, gas fraction) remains homogeneous. This directly recovers the empirically observed correlation between baryonic and dark mass profiles (23; 24), but here it arises naturally as a consequence of the gravitational field’s structure, rather than requiring a phenomenological assumption.

Thus, the hypothesis that dark mass is generated by gravitational potential energy not only accounts for its magnitude but also provides a fundamental explanation for its spatial distribution. What had previously appeared mysterious—the alignment between baryonic and dark matter—is shown here to be the logical consequence of field-based mass-energy equivalence.

Finally, this same gravitational potential energy makes it possible to create a functional dependence between galactic density and dark energy and to calculate it precisely. In addition, it offers a natural explanation for the emergence of negative pressure on cosmological scales. As gravitational interactions become progressively diluted with the increasing separation of structures, the macroscopic binding energy decreases—corresponding thermodynamically to an effective negative pressure. This pressure, derived directly from the evolution of the structured gravitational field, drives an accelerated expansion consistent with observations of dark energy. Thus, gravitational potential energy not only accounts for the dark mass but can also generate the repulsive effect that governs the large-scale dynamics of the universe.

The probability that these combined elements can explain the dark universe has been conservatively estimated at a significance level greater than 5σ. It should be emphasized that this estimate does not even consider the conceptual simplicity of the proposed model, nor the fact that gravitational potential energy is a well-established physical quantity, commonly used in engineering and classical physics. The idea that this energy could also play a real cosmological role gives this hypothesis an additional physical plausibility, independent of the correspondence to experimental data.

The Problem of the Epistemological Obstacle

Perhaps the most profound question raised by this work is why the role of gravitational potential energy in generating dark mass has remained unrecognized for so long. Both gravitational potential energy and the mass–energy equivalence relation $E = mc^2$ are well-established principles, each supported by extensive experimental validation. Moreover, the concept of binding energy contributing to mass is not new, nuclear binding energy, for example, is well

understood as a measurable mass defect in atomic systems, though its localization is typically attributed to the quantum field.

The primary reason gravitational binding energy has been historically dismissed as a source of mass is the perception that gravity is too weak a force to produce significant energy effects. However, our results challenge this assumption. While nuclear binding energy yields modest contributions to mass on the scale of atomic nuclei—often a few percent—gravitational potential energy can generate dark mass equivalents many times greater. In galactic systems, the ratio of gravitational potential energy to baryonic mass can exceed a factor of ten, and in clusters or larger structures, this ratio can be much higher.

This contrast highlights a scale-dependent truth; gravity is weak on the quantum scale but becomes dominant on astronomical scales, while the strong nuclear force behaves inversely. Immense at the subatomic level but negligible beyond the nucleus. The failure to account for this scale dependence may explain why the gravitational origin of dark mass has remained obscured despite the theoretical and empirical tools needed to uncover it.

Another major conceptual obstacle to recognizing the gravitational origin of dark mass lies in the widespread use of Newton's second theorem. Indeed, it allows a solid sphere to be considered as a point mass. This simplification naturally comes to mind when studying large stellar systems and has led to a poor understanding of what useful gravitational potential energy is. Traditional approaches focus on the relative position of celestial bodies, considered as point masses, emphasizing the term $E = -GmM / d$ as the main contribution. However, as we have demonstrated, this term is negligible compared to the energy associated with a restructuring of the system—for example, the merger or separation of massive bodies—under conservation of volume density.

The relevant potential energy does not result solely from distance, but from the energy difference between two distinct macroscopic states of the system. It is this transformation of state, respecting the physical properties of matter, that reveals the true energy content of the gravitational field. The historical focus on positional interaction, rather than on the internal reorganization of masses, has contributed to masking the role of potential energy as the real source of space-time curvature. By reconsidering potential energy as a quantity localized in the field and generating mass, we find a physically coherent explanation of the dark mass phenomenon—already contained in classical gravitational theory, but which has remained unnoticed due to a discreet but decisive conceptual bias.

Challenge of General Relativity and Theoretical Implications

A deeper theoretical difficulty lies in the fact that Newtonian gravity (GN) is not the fundamental theory of gravitation—General Relativity (GR) is. Unlike GN, GR does not admit a general, global conservation law for energy. As Emmy Noether showed, conservation of energy in GR only holds under very specific symmetries, such as time-translation invariance, which do not apply in dynamically evolving spacetimes. In particular, the notion of gravitational potential energy, central to Newtonian dynamics, does not have a direct, covariant analog in GR.

This creates a conceptual tension, if a phenomenon as significant as the dark mass arises from gravitational potential energy, and this energy is absent or ill-defined in GR, then one must ask why Newtonian theory—a weak-field approximation—appears to succeed where the full relativistic theory offers no equivalent formulation. The challenge is philosophical as well as physical.

Nevertheless, GN remains extraordinarily accurate in the weak-field regime and is vastly simpler to work with than GR. The dynamics of galaxies, where the gravitational field is weak and velocities are non-relativistic, fall squarely into this domain. In Newtonian gravity, the potential energy of the system is known, but to determine the correct dynamics, that energy must be reintroduced into the system—that is, it must be treated as a source of gravity. It is difficult to believe that GR would yield significantly better results unless the issue lies in an incomplete accounting of gravitational self-induction—the field's interaction with its own energy density (25; 26; 27; 28). If this is indeed the case, then the most natural resolution would be to find a weak-field expansion of GR in which this self-induction appears explicitly. In such a formulation, the gravitational potential energy term should re-emerge, but now as a derived, not postulated, quantity.

More speculatively, the fact that gravity *"recognizes"* all forms of energy—including gravitational potential energy, long regarded as a mere computational artifact—suggests the existence of a deeper unifying principle. The Higgs field already hints at such a principle in a limited domain, it translates scalar potential energy into inertial mass for

certain particles. Gravity appears to generalize this mechanism, coupling not just to scalar fields but to all forms of energy—kinetic, electromagnetic, nuclear, or gravitational.

The fundamental problem for coupling energy with other fields remains that energy is not conserved in GR. A striking example of this is the fact that potential energy is *"absorbed"* by black holes in our model. However, the non-existence of an invariance does not mean the non-existence of a phenomenon; on the contrary, it is even more interesting because of its variation. The problem amounts to introducing a variation into a physics based on invariance. Moreover, potential energy is a global phenomenon that is difficult to reconcile with a local phenomenon. Fortunately, renormalization is still there as a scaling adjustment mechanism.

Final Remarks

In conclusion, the study of dark mass does not seem to require an alternative theory of gravitation or exotic particles. Here, even general relativity seems superfluous; the framework of classical Newtonian mechanics, extended to the mass-energy equivalence $E = mc^2$, proves sufficient.

We have demonstrated that simple, physically grounded models can accurately reproduce the magnitude and distribution of dark mass in a wide range of galactic systems. These models can be systematically improved—for example, by incorporating a detailed synthesis of stellar populations, a more accurate treatment of interstellar gas, or a more refined modeling of radial distributions. The same methodology may also be extended to larger cosmic structures such as galaxy clusters and superclusters.

Furthermore, the mixed use of general relativity and classical calculation of potential energy seems necessary for a correct understanding of the phenomenon attributed to dark energy. Here too, an improvement of the model by a correct calculation of the average intergalactic distance seems necessary.

One conclusion is unavoidable, gravitational potential energy can no longer be neglected in in discussions on dark mass and dark energy. Its inclusion provides both a quantitative and conceptual solution to a long-standing astrophysical mystery.

The C++ and Python programs used to perform all numerical calculations and generate the corresponding graphs are freely available at dark-mass-generator.sourceforge.io.

Funding Statement

This research received no specific grant from any funding agency in the public, commercial, or not-for-profit sectors.

References

1. *Rotation of the Andromeda Nebula from a Spectroscopic Survey of Emission Regions.* **V. Cooper Rubin and W. K. Ford, Jr.** 1970, Astrophysical Journal, Vol. 159, p. 379.
2. *Rotational Properties of 21 Sc Galaxies with a Large Range of Luminosities and Radii from NGC 4605 (R=4kpc) to UGC 2885 (R=122kpc).* **V. Cooper Rubin, W. K. Ford, Jr. and N. Thonnard.** 1980, Astrophysical Journal, Vol. 238, p. 471.
3. *Rotation Velocities of 16 Sa Galaxies and a Comparison of Sa, Sb, and Sc Rotation Properties.* **V. Cooper Rubin, et al.** Astrophysical Journal, Vol. 289, p. 81.
4. *AGAPE: a Microlensing Search for Dark Matter by Monitoring Pixels.* **P. Gondolo, et al.** s.l. : ASP Conference Series (Dark and Visible Matter in Galaxies), 1997, Vol. 117.
5. *The MACHO Project: Microlensing Results from 5.7 Years of LMC Observations.* **C. Alcock, et al.** s.l. : Astrophysical Journal, 2000, Vol. 542, pp. 281-307.
6. *Limits on the Macho Content of the Galactic Halo from the EROS-2 Survey of the Magellanic Clouds.* **P. Tisserand, et al.** s.l. : Astronomy & Astrophysics, 2007, Vol. 469.
7. *Results from a search for dark matter in the complete LUX exposure.* **LUX Collaboration.** s.l. : Physical Review Letters, 2017, Vol. 118.
8. *Final results of the PICASSO dark matter search experiment.* **PICASSO Collaboration.** s.l. : Astroparticle Physics, 2017, Vol. 90, pp. 85-92. ISSN 0927-6505.
9. *Dark matter search results from the complete exposure of the PICO-60 C3F8 bubble chamber.* **PICO Collaboration .** s.l. : Physical Review D, 2019, Vol. 100.
10. *Search for low-mass dark matter via bremsstrahlung radiation and the Migdal effect in SuperCDMS.* **SuperCDMS Collaboration.** s.l. : Physical Review D, 2023.
11. *Probing Gravity at Cosmological Scales by Measurements which Test the Relationship between Gravitational Lensing and Matter Overdensity.* **Zhang, Pengjie, et al.** s.l. : Physical Review Letters, 2007, Vol. 99.
12. *Confirmation of general relativity on large scales from weak lensing and galaxy velocities.* **Reyes, Reinabelle, et al.** s.l. : Nature, 2010, Vol. 464, pp. 256–258.
13. *Strong Gravitational Lensing as a Probe of Dark Matter.* **Vegetti, S., et al.** s.l. : Space Science Reviews, 2024, Vol. 220.
14. *Microscope Mission: Final Results of the Test of the Equivalence Principle.* **MICROSCOPE Collaboration.** 2022, Physical Review Letters, Vol. 119.
15. *Transition from inspiral to plunge in binary black hole coalescences.* **Buonanno, Alessandra and Damour, Thibault .** 6, 2000, Physical Review D, Vol. 62.
16. *Gravitational-wave spectroscopy of massive black holes with the space interferometer LISA.* **Berti, Emanuele , Cardoso, Vitor and M. Will, Clifford.** 2006, Physical Review D, Vol. 73.
17. *Final spin from the coalescence of two black holes.* **Rezzolla, Luciano, et al.** 2008, Physical Review D, Vol. 78.
18. *Final mass and spin of black-hole mergers.* **Tichy , Wolfgang and Marronetti, Pedro .** 2008, Physical Review D, Vol. 78.
19. *The Black Hole Mass Function Across Cosmic Times. I. Stellar Black Holes and Light Seed Distribution.* **Sicilia, Alex , et al.** 2, 2022, The Astrophysical Journal, Vol. 924.
20. *SPARC: Mass Models for 175 Disk Galaxies with Spitzer Photometry and Accurate Rotation Curves.* **Lelli, Federico , McGaugh, Stacy S. and Schombert, James M.** 6, s.l. : The Astronomical Journal, 2016, Vol. 152, p. 157.
21. *L'énigme E = Mc2 : énergie potentielle et renormalisation de la masse.* **Brillouin, Léon.** 10, Paris : s.n., 1964, Journal de Physique, Vol. 25.
22. *The actual mass of potential energy, a correction to classical relativity.* **Brillouin, Léon.** 3, Proceedings of the National Academy of Sciences, Vol. 53.
23. *The Radial Acceleration Relation in Rotationally Supported Galaxies.* **McGaugh, Stacy S. , Lelli, Federico and Schombert, James M.** 2016, Physical Review Letters, Vol. 117.
24. *One Law to Rule Them All: The Radial Acceleration Relation of Galaxies.* **Lelli, Federico , et al.** 2, 2017, The Astrophysical Journal, Vol. 836, p. 152.
25. *An explanation for dark matter and dark energy consistent with the standard model of particle physics and General Relativity.* **Deur, Alexandre.** 2019, The European Physical Journal C, Vol. 79, p. 883.

26. *Significance of Gravitational Nonlinearities on the Dynamics of Disk Galaxies.* **Deur, Alexandre , Sargent, Corey and Terzić, Balša.** 94, s.l. : The Astrophysical Journal, 2020, Vol. 896.
27. *Effect of the field self-interaction of General Relativity on the cosmic microwave background anisotropies.* **Deur, Alexandre.** 13, s.l. : Classical and Quantum Gravity, 2022, Vol. 39.
28. *Relativistic corrections to the rotation curves of disk galaxies.* **Deur, Alexandre.** s.l. : The European Physical Journal C, 2021, The European Physical Journal C, Vol. 81, p. 213.